Dynamic Stabilization in The Double-Well Duffing Oscillator

Sang-Yoon Kim[1, *] and Youngtae Kim[2, †]
[1] *Department of Physics, Kangwon National University, Chunchon, Kangwon-Do 200-701, Korea*
[2] *Department of Physics, Ajou University, Suwon, Kyunggi-Do 442-749, Korea*

Bifurcations associated with stability of the saddle fixed point of the Poincaré map, arising from the unstable equilibrium point of the potential, are investigated in a forced Duffing oscillator with a double-well potential. One interesting behavior is the dynamic stabilization of the saddle fixed point. When the driving amplitude is increased through a threshold value, the saddle fixed point becomes stabilized via a pitchfork bifurcation. We note that this dynamic stabilization is similar to that of the inverted pendulum with a vertically oscillating suspension point. After the dynamic stabilization, the double-well Duffing oscillator behaves as the single-well Duffing oscillator, because the effect of the central potential barrier on the dynamics of the system becomes negligible.

PACS numbers: 05.45.-a

A periodically driven double-well Duffing oscillator [1], which has become a classic model for analysis of nonlinear phenomena, is investigated. It can be described in a normalized form by a second-order nonautonomous ordinary differential equations,

$$\ddot{x} + \gamma\dot{x} - x + x^3 = A\cos\omega t, \tag{1}$$

where γ is the damping coefficient, and A and ω are the amplitude and frequency of the external driving force, respectively.

The Duffing equation (1) with negative linear stiffness describes the dynamics of a buckled beam [2,3] as well as a plasma oscillator [4]. Its regular and chaotic dynamics has been analyzed in great details by Holmes using both the theoretical techniques and the computer simulations [2]. The results of this work have been also confirmed in experiments by Moon [3] for a buckeled elastic beam. Since then, a number of authors have studied the forced double-well Duffing oscillator in the past two decades, and found rich dynamical behaviors [1] such as the fractal basin boundary between coexisting competing attractors [5], hopping cross-well chaotic state [6], and so on.

Here we are interested in the dynamical behaviors associated with the saddle fixed point of the Poincaré map, arising from the unstable equilibrium point of the potential. One interesting behavior, associated with chaotic dynamics, is the homoclinic intersection of the stable and unstable manifolds of the saddle fixed point. In Ref. [2], Holmes showed that as the forcing amplitude A is increased the stable and unstable manifolds intersect transversally, giving rise to homoclinic motions. However, as A increases further, another interesting behavior, associated with stability of the saddle fixed point, occurs. When A passes through a threshold value, the saddle fixed point becomes stabilized via a pitchfork bifurcation. We note that the best-known example of this dynamic stabilization is the inverted pendulum with a vertically oscillating suspension point [7]. To our knowledge, this is the first report on such a dynamic stabilization in the double-well Duffing oscillator. After the dynamic stabilization, the behaviors of the double-well Duffing oscillator closely resembles those of the single-well Duffing oscillator [8], because the central barrier of the potential has no significant effect on the motion of the system.

For the numerical calculations we transform the second-order ordinary differential equation (1) into a system of two first-order ordinary differential equations:

$$\dot{x} = y,\ \dot{y} = -\gamma y + x - x^3 + A\cos\omega t. \tag{2}$$

These equations have a symmetry S, because the transformation

$$S : x \to -x,\ y \to -y,\ t \to t + \frac{T}{2}\ \ [T(\text{period}) = \frac{2\pi}{\omega}], \tag{3}$$

leaves Eq. (2) invariant. If an orbit $z(t)[\equiv (x(y), y(t))]$ is invariant under S, it is called a symmetric orbit. Otherwise, it is called an asymmetric orbit and has its "conjugate" orbit $Sz(t)$.

For the unforced case of $A = 0$, there exist a saddle equilibrium point at $(x, y) = (0, 0)$ and a conjugate pair of stable equilibrium points at $(x, y) = (\pm 1, 0)$. However, as A is increased from 0, one symmetric saddle-type orbit and two asymmetric attracting orbits with the same period $2\pi/\omega$ arise from the saddle equilibrium point and the two stable equilibrium points, respectively [2]. We note that they become the fixed points of the Poincaré map P, generated by stroboscopically sampling the orbit points with the external driving period T. Hereafter

*Electronic address: sykim@cc.kangwon.ac.kr
†Electronic address: ytkim@madang.ajou.ac.kr

we will denote the symmetirc saddle fixed point and the asymmetric stable fixed points by $z_{\rm s}^*$ and $z_{\rm a}^*$, respectively. Here we are interested in the bifurcations associated with stability of the symmetric saddle fixed point. Its linear stability is determined from the eigenvalues, called the Floquet multipliers, of the linearized Poincaré map DP, which can be obtained using the Floquet theory [9].

Since the Poincaré map P with a symmetry S has a constant Jacobian determinant (det) less than unity (det $DP = e^{-\gamma T}$), the only possible bifurcations of periodic orbits are saddle-node (SN), pitchfork (PF), and period-doubling (PD) bifurcations [10]. When a Floquet multiplier passes through 1, a PF or SN bifurcation takes place. On the other hand, when it passes through -1, a PD bifurcation occurs. Hopf bifurcations are excluded.

Each bifurcation curve in the parameter plane will be classified by a pair (p, q) invariant along the curve. Here q denotes the period of the orbit and p denotes the torsion number, which characterizes the average rotation number of the nearby orbits during the period q [11]. The torsion number (normalized by the factor 2π) at the PF or SN bifurcation curve becomes an integer. However, when crossing a PD bifurcation curve, not only the period but also the torsion number doubles from an odd multiple of $1/2$ to an odd integer. To keep p as an integer, we choose the pair of (p, q) for the PD bifurcation as that of the period-doubled orbit. We also note that the SN bifurcations may create symmetric and asymmetric orbits with the same (p, q). To differentiate them, their symmetries are also used to classify the SN bifurcations. For the case of the symmetric (asymmetric) orbit, a letter "s" ("a") will be added in the third entry such as [p, q, "s" ("a")] to label the corresponding "symmetric" ("asymmetric") SN bifrucation curve.

By varying the two parameters A and ω, we numerically investigate the bifurcation behavior associated with stability of the symmetric saddle fixed point for a moderately damped case of $\gamma = 0.1$. The associated bifurcation structure in the $\omega - A$ plane is shown in Fig. 1. Note that the region, hatched with vertical lines, is just the stability region of the symmetric saddle fixed point. It is bounded by a lower PF bifurcation curve PF(0,1), denoted by a dashed curve, and by an upper symmetric SN bifurcation curve SN(1,1,s), denoted by a dotted curve. When crossing the lower PF bifurcation curve PF(0,1), the saddle fixed point becomes stabilized through a PF bifurcation by absorbing a pair of asymmetirc fixed points. As a result of this dynamic stabilization, a symmetric stable orbit with period $2\pi/\omega$ (fixed point for the Poincaré map), encircling the unstable equilibrium point of the potential, appears. Note that this symmetric stabilized orbit corresponds to the symmetric stable orbit, arising from the stable equilibrium point of the potential in the single-well Duffing oscillator. Hence the dynamical behavior after such a dynamical stabilization becomes essentially the same as that of the single-well Duffing oscillator [8]. Such stabilized symmetric fixed point disappears at the upper symmetric SN bifurcation curve SN(1,1,s) by absorbing a symmetric unstable fixed point, born at the lower symmetric SN bifurcation curve SN(1,1,s).

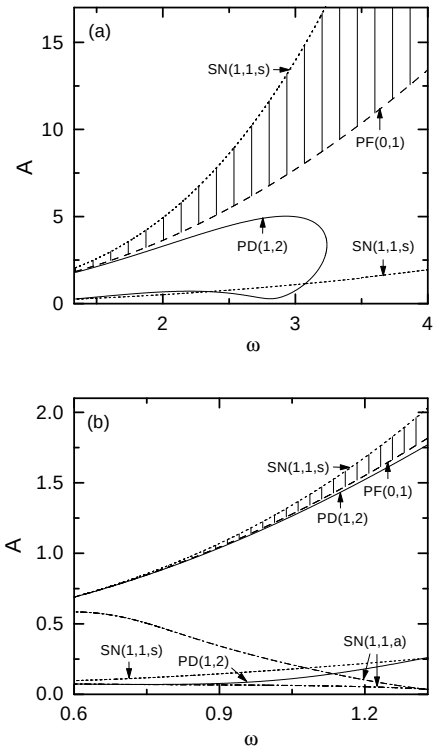

FIG. 1. Stability diagram of the symmetric saddle fixed point for (a) $\omega > \omega_{\rm r}(\simeq \sqrt{2})$ and (b) $\omega < \omega_{\rm r}$. The hatched region with vertical lines is just its stability region. The symbols SN, PF, and PD denote the saddle-node, pitchfork, and period-doubling bifurcation curves, respectively. Each curve is also labelled by a pair (p, q); p and q are the torsion number and period, respectively. To differentiate the symmetric and asymmetric SN bifurcations, the letters "s" and "a" are also added in the third entry such as [p,q,"s"("a")]. For other details, see the text.

For the unforced and undamped case, locally the Duffing oscillator near the two stable equilibrium points at $(x, y) = (\pm 1, 0)$ behaves as a soft spring with the natural frequency $\sqrt{2}$. Hence the main resonance occurs at $\omega = \omega_{\rm r}(\simeq \sqrt{2})$ in the linear limit. For $\omega > \omega_{\rm r}$ the symmetric saddle fixed point $z_{\rm s}^*$ becomes stabilized at the PF bifurcation curve PF(0,1) in Fig. 1(a) by absorbing a pair of asymmetric stable fixed points $z_{\rm a}^*$. However, for $\omega < \omega_{\rm r}$, the asymmetric stable fixed points $z_{\rm a}^*$ disappear at the upper asymmetric SN bifurcation curve SN(1,1,a), denoted by a dash-dotted curve in Fig. 1(b), through the collision with the asymmetric unstable fixed points born at the lower asymmetric SN bifurcation curve SN(1,1,a). After that, the symmetric saddle fixed point $z_{\rm s}^*$ becomes stable at the PF bifurcation curve PF(0,1) by absorbing a pair of asymmetric stable fixed points born at the lower asymmetric SN bifurcation curve SN(1,1,a), which will be denoted by $z_{\rm sn}^*$. We also note that the upper and lower asymmetric SN bifurcation curves form a "horn"

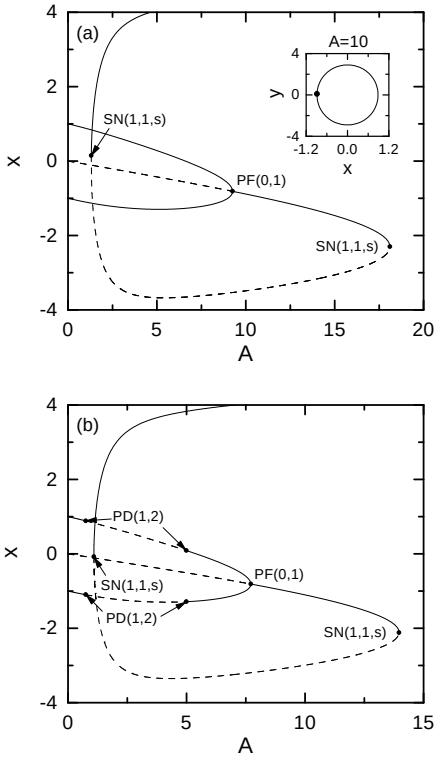

FIG. 2. Bifurcation diagrams (plots of x vs. A) for (a) $\omega = 3.3$ and (b) $\omega = 3.0$. Here the solid line denotes a stable fixed point, while the dashed line represent an unstable fixed point. The symbols denote the same as those in Fig. 1. The phase flow of the stabilized symmetric orbit for $A = 10$ is denoted by a solid curve in the inset in (a), and its Poincaré map is represented by a solid circle.

with a cusp at $\omega = \omega_{\rm r}$, as in the asymmetric Toda oscillator [12].

We now present the concrete examples of bifurcations associated with dynamic stabilization of the symmetric saddle fixed point. The bifurcation diagram and the phase-flow and Poincaré-map plots are also given for clear presentations of the associated bifurcations.

We first consider the case of $\omega > \omega_{\rm r}$. For $\omega = 2\omega_{\rm r}[\simeq 2\sqrt{2}]$, a subharmonic resonance occurs in which the asymmetric fixed points $z_{\rm a}^*$ become unstable by a PD bifurcation. Note that the PD bifurcation curve PD(1,2), belonging to the subharmonic resonance, becomes folded back at $\omega = \omega_{\rm f}(\simeq 3.23)$ [see Fig. 1 (a)]. Hence, when $\omega > \omega_{\rm f}$ no PD bifurcations occur for the asymmetric fixed points $z_{\rm a}^*$. As an example, we consider the case of $\omega = 3.3$. As shown in the bifurcation diagram in Fig. 2(a), the symmetric saddle fixed point $z_{\rm s}^*$ becomes stable through a PF bifurcation for $A = 9.255\cdots$ by absorbing a pair of asymmetric fixed points $z_{\rm a}^*$. Then a stabilized symmetric orbit, encirling the unstable equilibrium point of the potential, appears, which is shown for $A = 10$ in the inset in Fig. 2(a). After this dynamic stabilization, the dynamical behavior becomes similar to that of the single-well Duffing oscillator, because the effect of the central potential barrier on the dynamics of the system becomes negligible. Such a stabilized symmetric fixed point also disappears for $A = 18.105\cdots$ through a SN bifurcation by absorbing a symmetric unstable fixed point, born for $A = 1.309\cdots$ via a symmetric SN bifurcation.

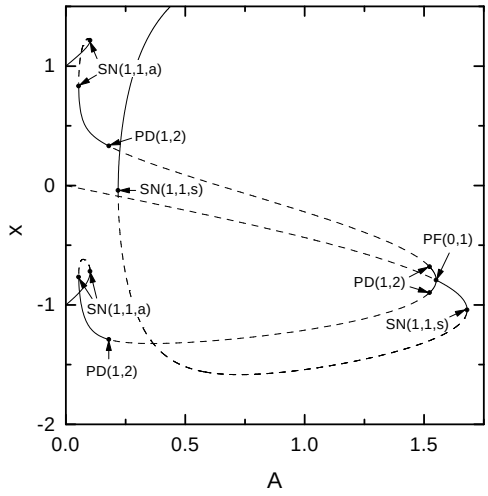

FIG. 3. Bifurcation diagram (plot of x vs. A) for $\omega = 1.2$. Here the solid line denotes a stable fixed point, while the dashed line represent an unstable fixed point. The symbols also denote the same as those in Fig. 1.

In the range of $\omega_{\rm r} < \omega < \omega_{\rm f}$, the mechanism of dynamic stabilization of the symmetric saddle fixed point is the same, except for the bifurcation behavior of the asymmetric fixed points $z_{\rm a}^*$. As an example, we consider the case of $\omega = 3.0$. As shown in Fig. 2(b), the asymmetric fixed points $z_{\rm a}^*$ lose their stability for $A = 0.748\cdots$ by forward PD bifurcations, but they become restabilized for $A = 4.991\cdots$ by backward PD bifurcations. Note that the subsequent bifurcations, associated with dynamic stabilization, are the same as those for the above case of $\omega = 3.3$.

We next consider the case of $\omega < \omega_{\rm r}$. An example for $\omega = 1.2$ is shown in Fig. 3. Unlike the case of $\omega > \omega_{\rm r}$, the asymmetric fixed points $z_{\rm a}^*$ disappear for $A = 0.101\cdots$ by the asymmetric SN bifurcations, and then jump phenomena occur in which the small asymmetric fixed points $z_{\rm a}^*$ are replaced by the relatively large asymmetric fixed points $z_{\rm sn}^*$, born for $A \simeq 0.053\,75$ via the asymmetric SN bifurcations. After that, the replaced asymmetric fixed points $z_{\rm sn}^*$ play the same role for the dynamic stabilization as the small asymmetric fixed points $z_{\rm a}^*$ do in the above case of $\omega > \omega_{\rm r}$. Hence the symmetric saddle fixed point $z_{\rm s}^*$ becomes stable via a PF bifurcation for $A = 1.550\cdots$ by absorbing $z_{\rm sn}^*$.

Finally, we discuss the bifurcation behavior of the double-well Duffing oscillator after the dynamic stabilization of the symmetric saddle fixed point. We note that the stabilized symmetric orbit, encircling the unstable equilibrium point of the potential, corresponds to

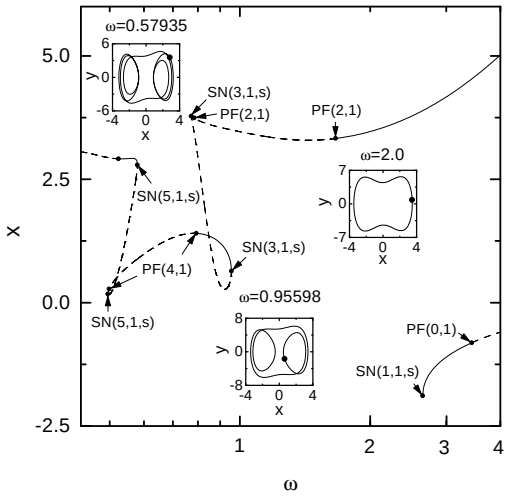

FIG. 4. Bifurcation diagram (plot of x vs. ω) for $A = 10$. Here the solid line denotes a stable fixed point, while the dashed line represent an unstable fixed point. The symbols also denote the same as those in Fig. 1. The phase portraits of the three large symmeric orbits, born by the symmetric SN bifurcations of type (1,1,s), (3,1,s) and (5,1,s), are shown for $\omega = 2.0$, $\omega = 0.95598$, and $\omega = 0.57935$, respectively.

the symmetric stable orbit, arising from the stable equilibrium point in the single-well Duffing oscillator. Consequently, the double-well Duffing oscillator behaves as the single-well Duffing oscillator, because the central potential barrier has no significant effect on the motion of the system. As an example, we present a bifurcation diagram (plot of x vs. ω) in Fig. 4, obtained by the frequency scanning for $A = 10$. The symmetric orbit stabilized through the PF bifurcation of type (0,1) disappears for $\omega = 2.646\cdots$ by a symmetric SN bifurcation of type (1,1,s), and then jumps to a large symmetric orbit born for $\omega = 9.306\cdots$ via a symmetric SN bifurcation of type (1,1,s). A phase portrait of the large symmetric orbit for $\omega = 2.0$ is shown in the inset. As ω is decreased, large symmetric orbits with higher odd torsion numbers p ($p = 3, 5, \ldots$), encircling the three equilibrium points of the potential, appear successively. The phase portraits of the large symmetric orbits with torsion numbers $p = 3, 5$ are given for $\omega = 0.955\,98$ and $0.579\,35$ in the insets, respectively. Note that the large symmetric orbits with higher torsion numbers have an increasing number of loops. Furthermore, each symmetric orbit with odd torsion number p loses its stability through a symmetry-breaking PF of type (p+1,1). Two such PF bifurcations of type $(2, 1)$ and $(4, 1)$ are also shown in Fig. 4. Then large asymmetric orbits with broken symmetry undergo period-doubling cascades. We note that all these bifurcation behaviors are essentially the same as those in the single-well Duffing oscillator (refer to Fig. 1 in Ref. [11]).

To confirm the above numerical results, we also constructed the electronic analog simulator of Eq. (1) with the usual operational amplifiers and multipliers, and made an analog study. Dynamic stabilization of the saddle fixed point was thus observed experimentally. The details on the experimental results will be given elsewhere [13].

ACKNOWLEDGMENTS

We would like to thank W. Lim for his assistance in the numerical computations. This work was supported by the Korea Research Foundation under Project No. 1998-015-D00065 (S.Y.K.) and 1998-015-D00060 (Y.K.) and by the Biomedlab Inc. (S.Y.K.).

[1] J. Guckenheimer and P. Holmes, *Nonlinear Oscillations, Dynamical Systems, and Bifurcations of Vector Fields* (Springer, New York, 1983), Sec. 2.2; F. C. Moon, *Chaotic and Fractal Dynamics* (Wiley, New York, 1992), Secs. 6.2 and 7.7.

[2] P. J. Holmes, Philo. Trans. R. Soc. London Ser. A **292**, 419 (1979).

[3] F. C. Moon and P. J. Holmes, J. Sound Vib. **65**, 275 (1979); F. C. Moon, ASME J. Appl. Mech. **47**, 638 (1980).

[4] R. A. Mahaffey, Phy. Fluid **19**, 1387 (1976).

[5] F. C. Moon and G.-X. Li, Phys. Rev. Lett. **55**, 1439 (1985).

[6] F. T. Arecchi and F. Lisi, Phys. Rev. Lett. **49**, 94 (1982); H. Ishii, H. Fujisaka, and M. Inoue, Phys. Lett. A **116**, 257 (1986).

[7] P. L. Kapitza, in *Collected Papers of P. L. Kapitza*, edited by D. Ter Haar (Pergamon, London, 1965), p. 714; S.-Y. Kim and B. Hu, Phys. Rev. E **58**, 3028 (1998).

[8] U. Parlitz and W. Lauterborn, Phys. Lett. A **107**, 351 (1985).

[9] J. Guckenheimer and P. Holmes, *Nonlinear Oscillations, Dynamical Systems, and Bifurcations of Vector Fields* (Springer-Verlag, New York, 1983), p. 24.

[10] J. Guckenheimer and P. Holmes, *Nonlinear Oscillations, Dynamical Systems, and Bifurcations of Vector Fields* (Springer-Verlag, New York, 1983), Sec. 3.5.

[11] U. Parlitz, Int. J. Bif. Chaos **3**, 703 (1993) and references therein.

[12] T. Kurz and W. Lauterborn, Phys. Rev. A **37**, 1029 (1988).

[13] Y. Kim, S.-Y. Lee, and S.-Y. Kim (to be published).